

# Transient Growth in Shear Flows: Linearity vs Nonlinearity

Chris C.T. Pringle\* and Rich R. Kerswell†  
*Department of Mathematics, University of Bristol,  
 University Walk, Bristol BS8 1TW, United Kingdom*  
 (Dated: October 31, 2018)

Two approaches to the problem of transition to turbulence of shear flows are popular in the literature. The first is the linear one of transient growth which focuses on the likely *form* of the most ‘dangerous’ (lowest energy) turbulence-triggering disturbances. The second is the nonlinear calculation of the laminar-turbulent boundary which instead focuses on their typical *amplitudes*. We look to bridge the gap between these two perspectives by considering the fully nonlinear transient growth problem to estimate both the form and amplitude of the most dangerous disturbance. We thereby discover a new nonlinear optimal disturbance which outgrows the well-known linear optimal for the same initial energy and is crucially much more efficient in triggering turbulence. The conclusion is then that the most dangerous disturbance can differ markedly from what traditional linear transient growth analysis predicts.

PACS numbers:

Shear flows are ubiquitous in nature and engineering, and understanding how and why they become turbulent has huge economic implications. This has led to a number of simplified canonical problems being studied such as plane Couette flow, channel flow and pipe flow which commonly exhibit turbulent behavior even when the underlying laminar state is linearly stable. In this case, a finite amplitude perturbation is required in order to trigger turbulence and a leading question is then what is the ‘most dangerous’ or ‘smallest’ such perturbation (with the metric typically being energy). Beyond its intrinsic interest, such information is fundamentally important for devising effective control strategies to delay the onset of turbulence.

Historically, linear transient growth analysis [1–5] has been used to identify dangerous disturbances which are efficient at triggering turbulence. This focuses on a linear mechanism whereby infinitesimally small perturbations can interact with the underlying shear profile in order to create much more energetic disturbances. Ultimately, these disturbances ebb away if the shear profile is linearly stable but the thinking is that the large growth possible can catapult the disturbance into a regime where nonlinear effects sustain its energy away from zero for all times.

Alternatively, recent progress has been made [6, 7] in numerically tracking the laminar-turbulent boundary which represents the surface in phase space which separates those initial conditions which will trigger a turbulent episode from those which will simply relaminarise. Since the tracking technique hinges upon carefully selecting initial conditions and integrating forward in time, the part of the boundary revealed is effectively confined to the neighborhood of the limiting set of the boundary-confined flow dynamics. This is found to have significantly higher energy levels than that actually needed to trigger turbulence by carefully-tuned initial disturbances

(e.g. [8]). This disparity in energy levels is none other than an expression of the large transient growth endemic in shear flows but now crucially translated into the nonlinear regime. The most dangerous disturbance corresponds with the minimum energy point on the laminar-turbulent boundary and stands to gain the largest energy as it sweeps up to the limiting set energy plateau. In this Letter, we pursue the promising strategy of extending the usual linear transient growth analysis into the nonlinear regime to identify the most dangerous disturbance in pipe flow. Our findings should be equally relevant to other shearing flows such as plane Couette flow, channel flow, boundary layers, etc.

The transient growth problem is the optimisation question: what initial condition  $\mathbf{u}(\mathbf{x}, t = 0)$  (added as a perturbation to the laminar flow  $2(1 - 4s^2)\hat{\mathbf{z}}$ ) for the governing Navier-Stokes equations with fixed (perturbation) kinetic energy  $E_0$  will give rise to the largest subsequent energy  $E_T$  at a time  $t = T$  later. This corresponds to maximising the functional

$$\begin{aligned} \mathcal{L} := & \langle \frac{1}{2}\mathbf{u}(\mathbf{x}, T)^2 \rangle - \lambda \langle \frac{1}{2}\mathbf{u}(\mathbf{x}, 0)^2 - E_0 \rangle \\ & - \int_0^T \langle \boldsymbol{\nu}, \left[ \frac{\partial \mathbf{u}}{\partial t} - 16su\hat{\mathbf{z}} + 2(1 - 4s^2)\frac{\partial \mathbf{u}}{\partial z} \right. \right. \\ & \quad \left. \left. + \mathbf{u} \cdot \nabla \mathbf{u} + \nabla p - \frac{1}{Re}\nabla^2 \mathbf{u} \right] \rangle dt \\ & - \int_0^T \langle \Pi \nabla \cdot \mathbf{u} \rangle dt - \int_0^T \Gamma \langle \mathbf{u} \cdot \hat{\mathbf{z}} \rangle dt \end{aligned} \quad (1)$$

where  $\langle \rangle$  represents volume integration;  $(s, \phi, z)$  are cylindrical coordinates directed along the pipe;  $\lambda$ ,  $\boldsymbol{\nu}(\mathbf{x}, t)$ ,  $\Pi(\mathbf{x}, t)$  and  $\Gamma(t)$  are Lagrange multipliers imposing the constraints of initial energy  $E_0$ , that the Navier-Stokes equations hold over  $t \in [0, T]$ , incompressibility and constant mass flux in time respectively (the system has been non-dimensionalised by the pipe diameter  $D$  and the bulk

velocity  $U$  with  $Re := \rho UD/\mu$  where  $\rho$  is the density and  $\mu$  is the dynamic viscosity). Vanishing of the variational derivatives requires that  $\mathbf{u}$  must evolve according to the Navier-Stokes equations,  $\boldsymbol{\nu}$  evolves according to the adjoint-Navier-Stokes equations and at times  $t = 0$  and  $T$  we have optimality and compatibility conditions linking the two sets of variables (e.g. see [9] for details of the linearised problem). The method of solution is one of iteration as follows:

- Make an initial guess for  $\mathbf{u}(\mathbf{x}, t = 0)$ .
- Allow  $\mathbf{u}(\mathbf{x}, t)$  to evolve according to the Navier-Stokes equations until  $t = T$ .
- Solve the compatibility condition for  $\boldsymbol{\nu}(\mathbf{x}, T)$ ,  $\delta\mathcal{L}/\delta\mathbf{u}(\mathbf{x}, T) \equiv \mathbf{u}(\mathbf{x}, T) - \boldsymbol{\nu}(\mathbf{x}, T) = \mathbf{0}$
- Allow the incompressible field  $\boldsymbol{\nu}(\mathbf{x}, t)$  to evolve *backwards* in time until  $t = 0$  via the adjoint-Navier-Stokes equations

$$\frac{\partial \boldsymbol{\nu}}{\partial t} + 2(1 - 4s^2)\frac{\partial \boldsymbol{\nu}}{\partial s} + \frac{1}{s}(\nu_\phi u_s - \nu_s u_\phi)\hat{\phi} + \mathbf{u} \cdot \nabla \boldsymbol{\nu} + 16s\nu_3\hat{s} + (u_i \partial_j \nu_i) = -\nabla \Pi - \frac{1}{Re} \nabla^2 \boldsymbol{\nu} \quad (2)$$

- Move  $\mathbf{u}(\mathbf{x}, 0)$  in the direction of the variational derivative  $\delta\mathcal{L}/\delta\mathbf{u}(\mathbf{x}, 0) \equiv -\lambda\mathbf{u}(\mathbf{x}, 0) + \boldsymbol{\nu}(\mathbf{x}, 0)$  and repeat.

Both direct and adjoint equations were solved using a fully spectral, primitive variables approach. Time stepping was done using a second order fractional step scheme, checked carefully against the code of [10]. The computational domain was a short periodic domain of length  $\pi$  radii with typical spatial resolution of 29 real Fourier modes azimuthally, 11 real Fourier modes axially and 25 modified Chebyshev polynomials radially in each of the 8 physical scalar fields ( $u, v, w, p, \nu_1, \nu_2, \nu_3, \Pi$ ). All results have been checked for robustness to resolution changes. Retention of the nonlinear terms poses a fresh technical challenge: although the adjoint equation is linear in  $\boldsymbol{\nu}$ , it is dependent on the evolution history of the forward variable  $\mathbf{u}$  which now must be stored.

The linear transient growth optimal  $\mathbf{u}_{lin}(\mathbf{x}; Re)$  in pipe flow is well-known to be streamwise-independent (2D) rolls which evolve into much larger streamwise-independent streaks [5]: see figs 1 and 2. Maximum growth occurs at  $T_{lin} \approx 12.2 \times Re/1000 (D/u)$  [11]. Introducing nonlinearity (ie increasing  $E_0$  from 0), setting  $T = 12.2 \times Re/1000 (D/U)$  and allowing only 2D flows, leads smoothly to a modified 2D optimal  $\mathbf{u}_{2D}(\mathbf{x}; E_0, Re)$  with monotonically decreasing growth (see [12] for an equivalent result in boundary layers). By  $E_0 \sim 10^{-3}$  (in units of the laminar flow's kinetic energy, used henceforth), the energy magnification falls to about 50% of its linear value at  $Re = 1750$ , and continues to decrease

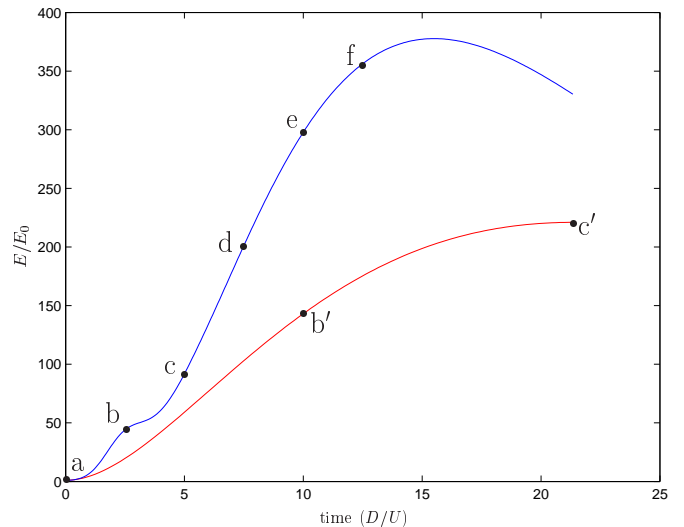


FIG. 1: The evolution of the linear and nonlinear optimals at  $Re = 1750$ . The blue line corresponds to the nonlinear optimal for  $E_0 = 2 \times 10^{-5}$  while the red line is the linear optimal ( $E_0 \rightarrow 0$ ). The nonlinear result produces more growth and actually reaches its maximum at a slightly earlier time than  $T$ .

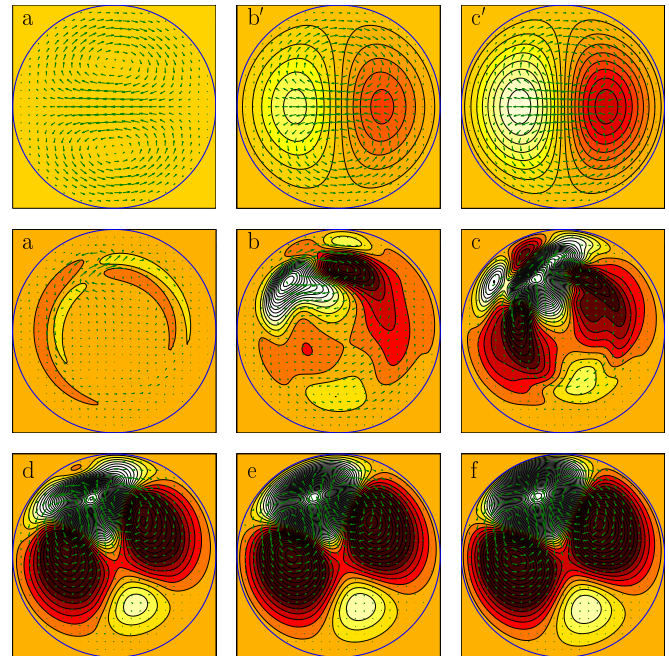


FIG. 2: Three snapshots of the linear optimal (top) and six snapshots (middle & bottom) of the 3D optimal for  $Re = 1750$  and  $E_0 = 2 \times 10^{-5}$  during its evolution. Labels refer to figure 1, arrows indicate cross-sectional velocities and colours axial velocity beyond the laminar flow (white/light for positive and red/dark for negative: outside shade represents zero).

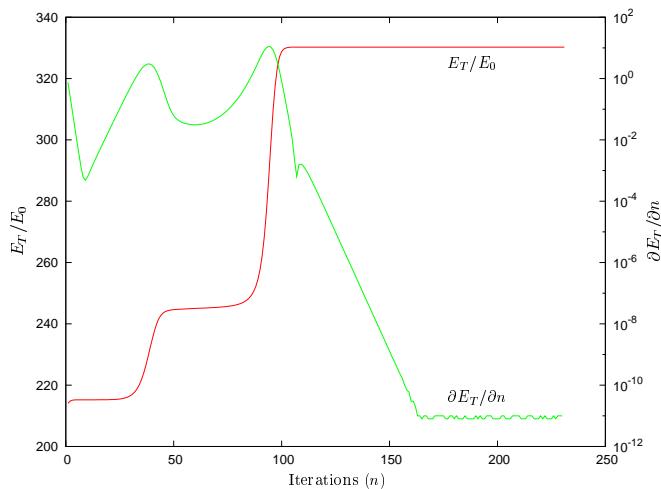


FIG. 3:  $Re = 1750$ ,  $E_0 = 2 \times 10^{-5}$ . The iterations are seeded with a noisy version of the 2D optimal and, after approaching two ‘saddle’ points, eventually converge onto the 3D optimal.

thereafter. Opening the optimisation up to fully 3D flows initially just recovers the 2D result but once  $E_0$  crosses a small threshold  $E_{3D}$  ( $\approx 10^{-5}$  at  $Re = 1750$ ), a completely new optimal  $\mathbf{u}_{3D}(\mathbf{x}; E_0, Re)$  appears. This new 3D optimal emerges from the optimisation procedure after it initially appears to converge to the 2D optimal and then transiently visits an intermediate state: see fig 3. Identifying this ‘loss of stability’ of the 2D optimal provided an efficient way to compute  $E_{3D}(Re)$ . All optimisation results were robust over three very different choices of starting flow: a)  $\mathbf{u}_{lin}$  with noise; b) the asymmetric travelling wave [13]; and c) a turbulent flow snapshot (all rescaled to the appropriate initial energy).

Given the intensity of the runs ( $O(200)$  iterations and each iteration requires integrating forwards and backwards over the period  $[0, T]$ ), we concentrated on two values of the Reynolds number,  $Re = 1750$  and  $2250$ , and the corresponding energy ranges  $[E_{3D} = 1.35 \times 10^{-5}, 2 \times 10^{-5}]$  and  $[E_{3D} = 4.8 \times 10^{-6}, 6.25 \times 10^{-6}]$ . Over both intervals the 3D optimal has essentially the same appearance: see fig. 2. Unlike the linear optimal which is globally simple in form and undergoes an evolution that is well established (rolls advecting the mean shear to generate streaks), the 3D optimal is localised to one side of the pipe and initially has both rolls and streaks of comparable amplitude. Figures 1 and 2 show a new 2-stage evolution: a preliminary phase when the flow delocalises followed by a longer growth phase where the flow structure stabilises to essentially two large-scale slow streaks sandwiching one fast streak near the boundary.

If  $E_0$  is increased beyond the ranges quoted above, the iterative procedure fails to converge for reasons which are unclear. One possibility is that at these energy levels, the laminar-turbulent boundary has been crossed and

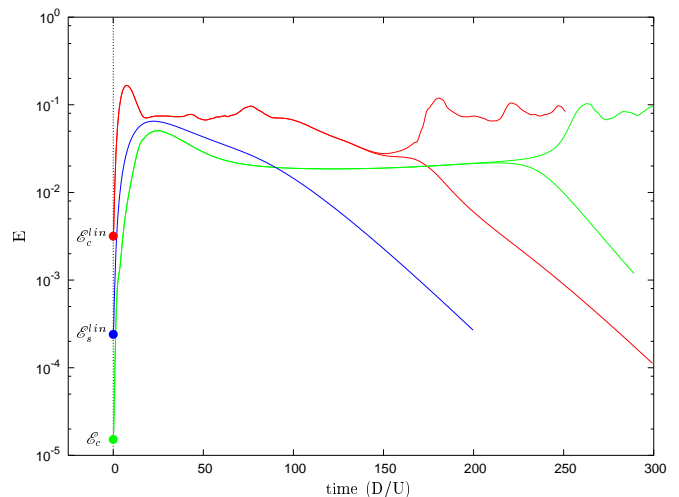


FIG. 4:  $Re=2500$ . The green line shows the evolution of the 3D optimal when given initial energy  $\mathcal{E}_c$ . Because it is on the laminar-turbulent boundary two nearly identical initial conditions diverge after, in this case,  $220D/U$ . The blue line is the evolution of the 2D optimal for the exact initial energy  $\mathcal{E}_s^{lin}$  for which the streaks become linearly unstable. The red line shows the 2D optimal given initial energy  $\mathcal{E}_c^{lin}$  and allowed to evolve until it reaches a maximum amplitude whereupon 0.1% by amplitude unstable perturbation is added. Again the laminar-turbulent boundary can be identified.

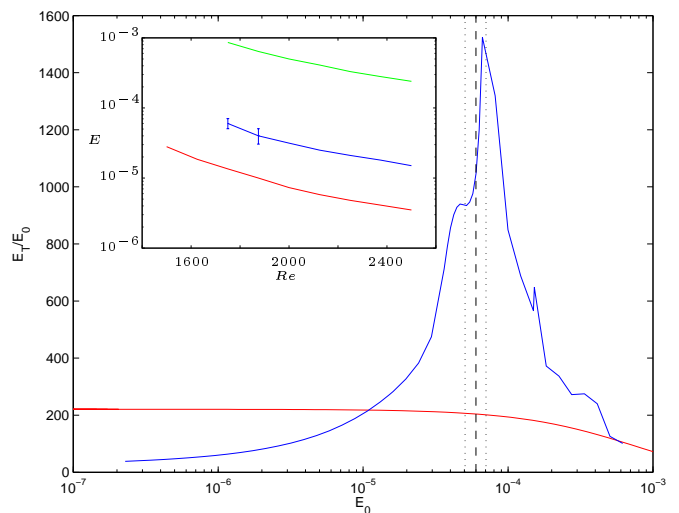


FIG. 5: The effect of the initial energy on the growth of  $\mathbf{A}\mathbf{u}_{lin}$  (red) and  $\mathbf{A}\mathbf{u}_{3D}$  (blue) at  $Re = 1750$ . For small  $E_0$  the 2D result is the optimal but after  $E_{3D} = 1.35 \times 10^{-5}$ , the 3D optimal takes over. The vertical dashed line corresponds to  $\mathcal{E}_c$ , with the dotted lines being the relevant errorbars. **Inset:** The dependence of  $E_{3D}$  (red),  $\mathcal{E}_c$  (blue) and  $\mathcal{E}_s^{lin}$  (green) on  $Re$  ( $\mathcal{E}_c^{lin}$  is even higher). The error bars shown on  $\mathcal{E}_c$  at  $Re = 1750$  and  $1875$  are because the laminar-turbulent boundary is difficult to identify at these  $Re$  due to the pipe shortness.

the lack of convergence is due to the flow becoming turbulent. The ensuing sensitivity to noise would make the optimisation non-smooth. However, direct numerical simulation starting with the 3D optimal does not reveal a turbulent episode implying that there is still an energy gap between where the 3D optimal emerges as the solution to the transient growth problem and the lowest energy of any initial condition which can trigger turbulence [15]. What can be shown, however, is that the 3D optimal is much more efficient at triggering turbulence than the linear optimal when rescaled. Taking the initial condition  $\mathbf{A}u_{3D}(\mathbf{x}; 2 \times 10^{-5}, 1750)$ , we gradually increase the rescaling factor  $A$  until a critical energy  $E_0 = \mathcal{E}_c(Re)$  is reached at which turbulence is triggered. Calculating the corresponding quantity for the linear optimal turns out to be less clearly defined because some 3D noise is needed to trigger turbulence. As a result we make 2 different estimates, one strictly conservative and the other more realistic. The first  $\mathcal{E}_s^{lin}$  is obtained by taking  $\mathbf{A}u_{lin}(\mathbf{x}; 1750)$  and finding the initial energy for which the resultant streaks are just linearly unstable in this periodic domain [14]. In the second  $\mathcal{E}_c^{lin}$ , the same initial condition was used but 0.1% of the most unstable perturbation (as found from the previous computation) is added to the streaks when they reach maximum amplitude.  $\mathcal{E}_s^{lin}$  should be a (low) conservative estimate but even this is O(10) times larger than  $\mathcal{E}_c$  at  $Re = 2500$  - see figure 4 - whereas the more realistic  $\mathcal{E}_c^{lin}$  is O(100) times larger.

In figure 5(inset) we plot  $E_{3D}$ ,  $\mathcal{E}_c$  and  $\mathcal{E}_s^{lin}$  as a function of  $Re$  which emphasizes that the 2D optimal (for which the linear result is an excellent approximation) ceases to be a global maximum at an energy (at least) several orders of magnitude before it approaches the laminar-turbulent boundary. The 3D optimal, in contrast, crosses the laminar-turbulent boundary only shortly after it emerges at  $E_{3D}$ . This indicates that the 3D optimal provides a rapid means of bridging the gap between when the 3D nonlinear optimal surpasses the linear result and when turbulence can be triggered. To achieve this, the energy growth experienced by the 3D optimal must increase dramatically with  $E_0$  which is illustrated in figure 5. It is worth remarking that the lowest possible energy to trigger turbulence must be bounded below by  $E_{3D}$  [15] and above by  $\mathcal{E}_c$ .

In this letter we have demonstrated that including nonlinearities in the problem of transient growth critically changes the result close to the onset of turbulence. Although we have not been able to calculate these solutions all the way up to the laminar-turbulent boundary as originally hoped, we provide evidence that they are very efficient at triggering turbulent episodes, notably more so than the linear result. Admittedly, we have only considered a short periodic domain and so the natural question is what will happen in larger domains. Here we expect further localisation of the optimal since en-

ergy is defined as a *global* quantity whereas nonlinearity is important wherever the velocity field is *locally* large. This strongly suggests that in a long pipe the optimal should localise in the axial direction as well (the 3D optimal found here is already localised in the radial and azimuthal directions). This squares well with the experimental observation that small local perturbations can trigger high energy global turbulence. More importantly, the fact that localised flow structures should emerge from this type of theoretical analysis bodes well for a greater connection between theory and experiments which naturally introduce localised disturbances.

Finding fully nonlinear optimals is a time-consuming pursuit due to the slow convergence of the iterative procedure and the need to look within small energy windows. Their discovery has had to wait almost two decades after the linear result was established in pipe flow. As computer power steadily increases, we envision that these new nonlinear optimals will start to come within easy reach. That the optimal found here represents something entirely different to the previously known linear results suggests that they will open up a whole new means of triggering turbulence and a whole new way of understanding how transition occurs.

The calculations in this paper were carried out at the Advanced Computing Research Centre, University of Bristol.

---

\* Electronic address: C.C.T.Pringle@reading.ac.uk

† Electronic address: R.R.Kerswell@bristol.ac.uk

- [1] L.H. Gustavsson, J. Fluid Mech. **224**, 241 (1991).
- [2] K.M. Butler, B.F. Farrell, Phys. Fluids A **4**, 1637 (1992).
- [3] L. Bergström, Stud. Appl. Maths **87**, 61 (1992).
- [4] L.N. Trefethen *et al.*, Science **261**, 5121 (1993).
- [5] P.J. Schmid, D.S. Henningson, J. Fluid Mech. **277**, 197 (1994).
- [6] T. Itano, S. Toh, J. Phys. Soc. Jpn. **70**, 703 (2001).
- [7] T.M. Schneider, B. Eckhardt, and J.A. Yorke, Phys. Rev. Lett. **99**, 034502 (2007).
- [8] D. Viswanath, P. Cvitanovic, J. Fluid Mech. **627**, 215 (2009).
- [9] A. Guégan, P.J. Schmid and P. Huerre, J. Fluid Mech. **566**, 11 (2006).
- [10] A.P. Willis, R.R. Kerswell, J. Fluid Mech. **619**, 213 (2009).
- [11] A. Meseguer, L.N. Trefethen, J. Comp. Phys. **186**, 178 (2003).
- [12] S. Zuccher, A. Bottaro, P. Luchini, Eur. J. Mech. B, **25**, 1 (2006).
- [13] C.C.T. Pringle, R.R. Kerswell, Phys. Rev. Lett. **99**, 074502 (2007).
- [14] S.C. Reddy *et al.*, J. Fluid Mech. **365**, 269 (1998).
- [15] There is the assumption that the optimisation algorithm samples all possible flows of a given energy and thus if it converges smoothly, turbulence cannot be triggered at this energy level.